Available online at www.sciencedirect.com
ScienceDirect
Journal of the European Ceramic Society 27 (2007) 4575–4588
www.elsevier.com/locate/jeurceramsoc

BAS, CMAS and CZAS glass coatings deposited by plasma spraying

G. Bolelli, L. Lusvarghi *, T. Manfredini, E. Parsini, C. Siligardi

Dipartimento di Ingegneria dei Materiali e dell'Ambiente, University of Modena and Reggio Emilia, Via Vignolese, 905, 41100 Modena, Italy

Received 20 January 2007; received in revised form 7 March 2007; accepted 16 March 2007
Available online 29 May 2007

Abstract

In this study, three different industrial frits $BaO–Al_2O_3–SiO_2$ (BAS), $CaO–MgO–Al_2O_3–SiO_2$ (CMAS), $CaO–ZrO_2–Al_2O_3–SiO_2$ (CZAS) have been deposited on porcelainized stoneware tiles by plasma spraying. In the as-sprayed conditions, the microstructure of the coatings is defective because of pores, microcracks and low intersplat cohesion. Hot stage microscope and differential thermal analysis measurements made on the glass powders allowed to characterize the frits thermal behaviour. Post process thermal treatments have been arranged, following these indications as well as preliminary tests, in order to achieve the lowest porosity and the highest resistance to abrasion. At the chosen temperatures, a microstructural improvement has been induced, but in the BAS specimens, an optimal sintering has not been accomplished because of the unavoidable full overlapping of the sintering and crystallization processes.

Keywords: Plasma-spraying; Sintering; Glass ceramics; Mechanical properties

1. Introduction

All traditional glazing techniques involve application of a slip on a green (single-firing) or on a fired body (double firing) and the firing of the glaze + substrate system.[1] This implies two main drawbacks: the requirement of glazes with the same firing temperature and almost the same thermal expansion coefficient as the substrate. These requirements impose limits on glazes compositions, preventing the adoption of systems with high mechanical properties: in fact, common glazes have poorer superficial mechanical properties than unglazed porcelanized stoneware. In plasma spraying, instead, the substrate is only moderately pre-heated, and should a post-process thermal treatment be needed, the temperature would be significantly lower than that of traditional firing processes.[2] So, thermal incompatibility troubles are greatly lessened.

A plasma torch consists of a tungsten cathode, a water-cooled copper anode with a central nozzle, and a gas feeding system; an arc is struck between the cathode and the anode, across the gas flux, so that ionization of atoms and molecules transform the gas into a hot (up to 14,727 °C) and high-velocity plasma.[3] The coating material, in powder form, is radially fed into the plasma flux just outside the nozzle exit: the particles are therefore dragged and heated by the plasma itself, so that they melt and accelerate towards the substrate. The melted droplets impact on the substrate, flattening and solidifying in a few microseconds, assuming a typical lamellar (or splat-like) morphology. Among thermal spraying techniques, the plasma-spraying is probably the fittest to spray glass powders. However, plasma-spraying has seldom been tested with glasses, except for a few cases, especially in the biomedical field.[4–7] Recently, further studies on plasma sprayed glasses have been performed from the point of view of the mechanical properties, both in composite coatings with alumina as reinforcement,[8–11] and as glaze substitutes on traditional ceramics substrates.[2,12] The latter research concerned an industrial high quality glass composition based on the $CaO–ZrO_2–SiO_2$ (CZS) system. Thanks to the viscous properties and thermal behaviour of the glass, the results were very promising, notwithstanding the need of a post deposition heat treatment due to the poor microstructure of the as-sprayed specimens.

The aim of this paper is to investigate three plasma sprayed industrial glass frits, which can act as glazes on stoneware tiles, and to check which properties of the base glass compositions are required to achieve a good sintering and crystallization of the coatings by means of a post process thermal treatment. For sake

* Corresponding author. Tel.: +39 0592056206; fax: +39 0592056243.
E-mail address: lucalusv@unimore.it (L. Lusvarghi).

0955-2219/$ – see front matter © 2007 Elsevier Ltd. All rights reserved.
doi:10.1016/j.jeurceramsoc.2007.03.032

Table 1
Chemical composition of industrial frits

Frit	Oxides (wt%)
BAS	40.0% BaO, 18.3% Al_2O_3, 41.7% SiO_2
CMAS	23.3% CaO, 9.2% MgO, 19.3% Al_2O_3, 47.7% SiO_2 and 0.5% K_2O
CZAS	25.9% CaO, 12.9% ZrO_2, 13.8% Al_2O_3, 47.4% SiO_2

Table 2
Critical temperatures of the frits

Frit	T_g (±2 °C)	T_c (±2 °C)	T_{sint} (±2 °C)
BAS	630	778	830
CMAS	735	910	884
CZAS	790	$T_{c1} = 1037$; $T_{c2} = 1127$	900

of comparison, microhardness, toughness and abrasion resistance have been investigated also on unglazed porcelainized stoneware tiles and on a high quality industrial glaze made of a glassy matrix reinforced with corundum grains.

2. Experimental procedure

2.1. Powders production and characterization

Three industrial frits expressly designed for devitrification (Colorobbia ITALIA, S.p.A., Italy), whose nominal chemical composition is listed in Table 1, have been employed in this study. Plasma sprayed coatings properties strongly depend on the powder size distribution.[13] Keeping the other process parameters fixed, a higher average diameter of the particles usually causes a higher amount of porosity in the coating and vice versa. Thus, the frits have been intensively ball milled (sintered alumina balls). Measurements of the average diameter were performed in water (Laser Size Analyser, Malvern Instruments, Malvern, Worcestershire, United Kingdom). On the other hand, very fine crushed powders possess a poor flowability, leading to possible stops of the spraying due to clogs in the feeder system. For this reason, they have been subsequently spray dried (NERO Atomizer, Denmark) to get a spherical shape; in this case the measurements of average diameter were performed in dry conditions. Tap density measurements (DENSI-TAP IG/4, MA.TEC. Giuliani, Torino, Italy) were performed to assess the flowability improvement considering the compressibility index (C.I. = $[(V_i - V_f) \times 100)/V_i]$, where V_i and V_f are the initial volume of the powder and the final volume after the test, respectively) as main parameter according to the ASTM D4164 standard. Scanning electron microscopy (SEM, XL-30, FEI, Eindhoven, The Netherlands, equipped with energy dispersive spectrometer, EDS) and X-ray powders Diffractometry (XRD, PW 3710, Philips, Cu Kα radiation) have been used to study the powder shape and crystallinity. Differential thermal analysis (DSC 404, Netzsch-Gerätebau, Selb/Bavaria, Germany) has been performed to obtain the critical temperatures of the frits, such as glass transition and crystallization temperature (T_g, T_c); besides, sintering tests on pressed powder have been carried out with a hot stage microscope (Misura HSM ODHT, Expert System Solutions, Modena, Italy) to find the sintering temperature (T_{sint}) for the three frits (Table 2).

2.2. Coating manufacturing

Plasma-spraying runs have been performed at Centro Sviluppo Materiali (Roma, Italy) using CAPS (Controlled Atmosphere Plasma Spray, shared with Università 'La Sapienza', Roma) system equipped with an F4-MB torch, in Atmospheric Plasma Spraying (APS) mode, using operating parameters listed in Table 3. Substrates were unglazed porcelanized stoneware tiles grit blasted with 500 μm alumina particles before deposition. Depositions with the same spraying parameters, but with a torch single pass, were also performed in order to investigate the single splats and correlate their properties and morphology to the properties of the coatings. Single splats have been deposited on a polished glass substrate because the very low roughness of this material allows a better observation of splats morphology than a porcelanized stoneware substrate, whose average roughness is always higher than 1 μm.

2.3. Coating characterization

The plasma sprayed coatings characterization was carried out with XRD and scanning electronic microscopy on polished cross-sections (mounted in resin, ground with 400, 800, 1000, 2000 mesh SiC papers and polished with 3 and 0.5 μm poly-crystalline diamond suspension). Image analysis was also performed on 400× backscattered SEM images to determine coating porosity (three images have been examined for each kind of coatings; UTHSCSA Image Tool v. 3.0 software).

Table 3
Spraying parameters for the glass coatings (A) and the single splats experiment (B)

Parameters	BAS	CMAS	CZAS
Nozzle	$d = 6$ mm	$d = 6$ mm	$d = 6$ mm
Power	38.9 kW	38.6 kW	38.1 kW
Spraying distance	100 mm	100 mm	100 mm
Carrier gas	Ar 3.5 slpm	Ar 3.5 slpm	Ar 3.5 slpm
Plasma gas	Ar 45 slpm + H_2 14 slpm	Ar 50 slpm + H_2 15 slpm	Ar 50 slpm + H_2 16 slpm
Number of passes	(A) 10 pre-heating and 60 spraying; (B) 3 pre-heating and 1 spraying	(A) 5 pre-heating and 55 spraying; (B) 3 pre-heating and 1 spraying	(A) 5 pre-heating and 50 spraying; (B) 3 pre-heating and 1 spraying
Cooling system	Ar, 7 bar	Ar, 8.5 bar	Ar, 8 bar

Roughness measurement was performed by mechanical profilometry (RUPAC, TR-200, Milano, Italy), determining the R_a parameter (UNI ISO 4287-1).In order to assess the micromechanical properties of the coatings, Vickers microhardness (Open Platform, CSM Instruments, Switzerland; 15 indentations, loading time 15 s, load = 0.25 N) on cross-sections and indentation fracture toughness (10 Vickers indentations, loading time 15 s, load = 2 N), measuring the cracks lengths through optical microscopy and employing in the calculations the Evans–Charles[14] (1.1) and Evans–Wilshaw[15] (1.2) formulae

$$K_{IC} = 0.0824 \times \frac{P}{c^{3/2}} \quad (1.1)$$

$$K_{IC} = 0.079 \times \left(\frac{P}{a^{3/2}}\right) \times \log\left(\frac{4.5a}{c}\right) \quad (1.2)$$

where $K_{IC} = MPa \times m^{0.5}$, a is the half diagonal of the indentation (μm), c the crack length (μm), and P is the load (mN)), have been evaluated on the specimens. A simple dry sand-steel wheel test, using a 200.1 mm diameter Fe360A steel wheel rotating at 75 rpm, FEPA 80 alumina grains (180 μm average particle diameter) as abrasive medium with a 1 g/lap mass flux, and applying a 40.2 N normal load (Ceramic Instruments AP/87 abrasimeter, Sassuolo, Italy), with results expressed as the ratio between the wear volume in mm^3 and the sliding distance in mm, has been performed to measure the abrasion resistance of the plasma sprayed coatings (six wear tracks for each sample after 7, 14 and 21 disk revolutions). This ratio has been labelled with V_{mm} when representative of the test outcomes after 7 wheel revolutions and with V_{mm} average, when regarding the mean of the values measured after 7, 14 and 21 revolutions.

2.4. Post-process heat treatments

In order to improve the microstructure and mechanical properties of the as-sprayed coatings, thermal treatments in an electric kiln have been performed on BAS, CMAS and CZAS coatings in order to induce sintering and crystallization. As demonstrated in previous works,[2,12] a thermal treatment is necessary to enhance the microstructure of the coatings, i.e. to sinter the glass. To fully induce an overall improvement of the properties, as already experimentally determined in the CZS case,[2,12] the heat treatment should also be able to transform the layer from a glass to a glass ceramic material, i.e. induce the nucleation and growth of crystals from the base glass through the whole thickness of the coating. The latter requirement should be potentially fulfilled, if surface crystallization is the main process occurring in the glass coating, because pores, interfaces, microcracks and all the "free-surfaces" of the as-sprayed layers should act as heterogeneous nucleation sites, allowing a complete devitrification of the coating. Thus, a double isotherm thermal treatment should perform both tasks: the first isotherm at T_{step1} is a "sintering step", whose aim is closing cracks and connected porosity; the second isotherm at T_{step2} is a "crystallization step", whose purpose is changing the nature of the coating (from vitreous to crystalline). To better understand the evolution of the changes caused in the coatings by the heat treatments, the samples have been investigated both after one single isotherm at T_{step1}, and after a complete double isotherm first at T_{step1} and then at T_{step2} (labelled as $T_{step1} + T_{step2}$). In order to choose the isotherm temperatures (T_{step1}, T_{step2}) and suitable soaking times, many preliminary heat treatments on the coatings have been performed. The samples have been subsequently characterized in order to find the ones, which underwent an optimal sintering (lowest amount of porosity and number of microcracks) and crystallization (largest number of crystals widespread through the coating thickness) process. In some cases, T_{step1} and T_{step2} did not coincide with the critical temperatures (T_{sint}, T_c) of the correspondent glass compositions (Table 4): such discrepancy is probably caused by some unavoidable differences between the conditions (kiln chamber much bigger than DTA furnace, different sample size, etc.) in which the experiments on the glass powders and coatings have been executed. The same kind of characterization performed on the as-deposited coatings has been carried also on the heat-treated samples.

2.5. Bulk sample characterization

In order to get further information on the properties of the glasses and glass ceramics, bulk glasses and sintered samples have been investigated. Bulk glass samples were obtained by melting the glass powders in platinum crucibles and casting them into graphite moulds. They have also undergone annealing treatments in order to relax internal stress induced by fast cooling. Dilatometry has been performed on bars 15 mm × 5 mm × 5 mm obtained from bulk samples by cutting and grinding. A crystallization study has been performed on bulk samples: crystallization isotherms were performed at T_{step2} for CMAS and BAS samples and at T_{c1} for CZAS. In all cases, the rate of heating was 10 °C/min, 30 min isotherm. Samples were cooled to room temperature inside the kiln after heat treatments. Heat treated samples surface and cross section were observed by means of a SEM. XRD was also performed on the surfaces of the samples to study the crystalline phases formed by thermal treatments. The crystallization study has been also carried out on sintered samples: the powders were wetted with 5 wt%

Table 4
Details of the thermal treatments

Composition/heat treatment	Sintering step (T_{step1}) (10 °C/min)	Sintering step + crystallization step ($T_{step1} + T_{step2}$) (10 °C/min)
BAS	Single isotherm at 778 °C for 30 min	Double isotherm at 778 °C for 30 min + 830 °C for 30 min
CMAS	Single isotherm at 850 °C for 60 min	Double isotherm at 850 °C for 60 min + 967 °C for 30 min
CZAS	Single isotherm at 900 °C for 60 min	Double isotherm at 900 °C for 60 min + 950 °C flash[a]

[a] Since the crystallization process was detrimental to the coating microstructure (Section 3.4.2) the furnace was switched off once reached T_{step2}.

of distilled water and uniaxially pressed in 40 mm diameter disks under 40 MPa load. The pressed disks were sintered and crystallized in an electric kiln, using the same thermal cycles described in Table 4 for thermally treated plasma sprayed coatings. Cross sectional samples from sintered disks were observed through SEM and their surfaces were subjected to XRD. Vickers microhardness and indentation fracture toughness have also been measured on the bulk and sintered samples in the same experimental conditions described above.

3. Results and discussion

3.1. Powders characterization

All powders studied show a monomodal distribution and the average diameter was in all cases ~10 μm for ball milled powders and ~15 μm for spray dried powders. The difference in their size distribution can be seen in Fig. 1. Ball-milled and spray-dried powder morphologies are quite different, in particular, as can be seen in Fig. 2, the milled powder is composed by small particles with irregular, angular shape, whereas, in the spray-dried case, the fine particles are agglomerated in spherical-shaped aggregates, enhancing the powder flowability. The tap-density analysis confirmed the enhancement of the powder flowability after spray drying having found a decreasing of the C.I. in all cases: BAS, $C.I._{crushed} = (30.1 \pm 1.9)$, $C.I._{spray\ dried} = (23.5 \pm 0.5)$; CMAS, $C.I._{crushed} = (28.2 \pm 3.9)$, $C.I._{spray\ dried} = (21.1 \pm 0.2)$; CZAS, $C.I._{crushed} = (28.0 \pm 2.3)$, $C.I._{spray\ dried} = (22.4 \pm 0.6)$. Differential thermal analysis data (Table 2) indicate that all three frits show a clear crystallization peak, CZAS a second one at higher temperature. In Table 2, the highest sintering rate temperatures (T_{sint}) for the three compositions obtained by sintering tests on pressed powders are also shown. X-ray patterns revealed that CMAS and CZAS frits are completely glassy, instead BAS pattern shows some low intensity peaks relating to hexacelsian phase ($Ba_{0.808}(Al_{1.71}Si_{2.29})O_8$ JCPDS 088-1050).

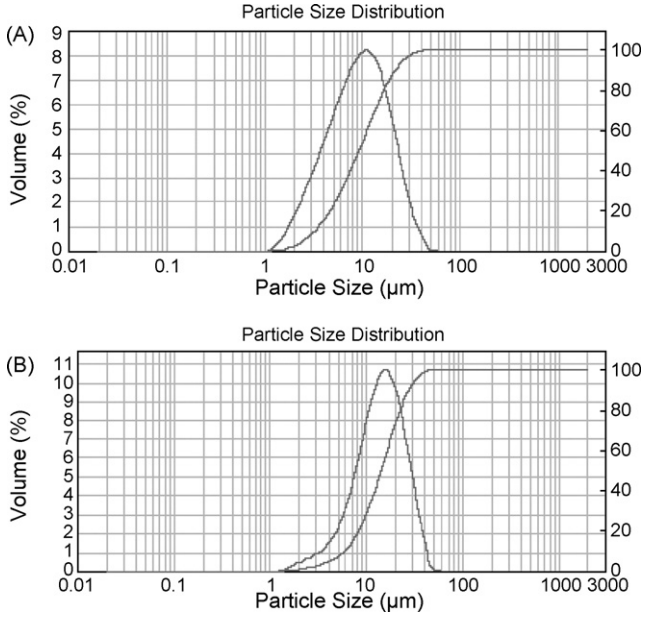

Fig. 1. Particle size distribution for CMAS: (A) ball-milled powder and (B) spray dried powder.

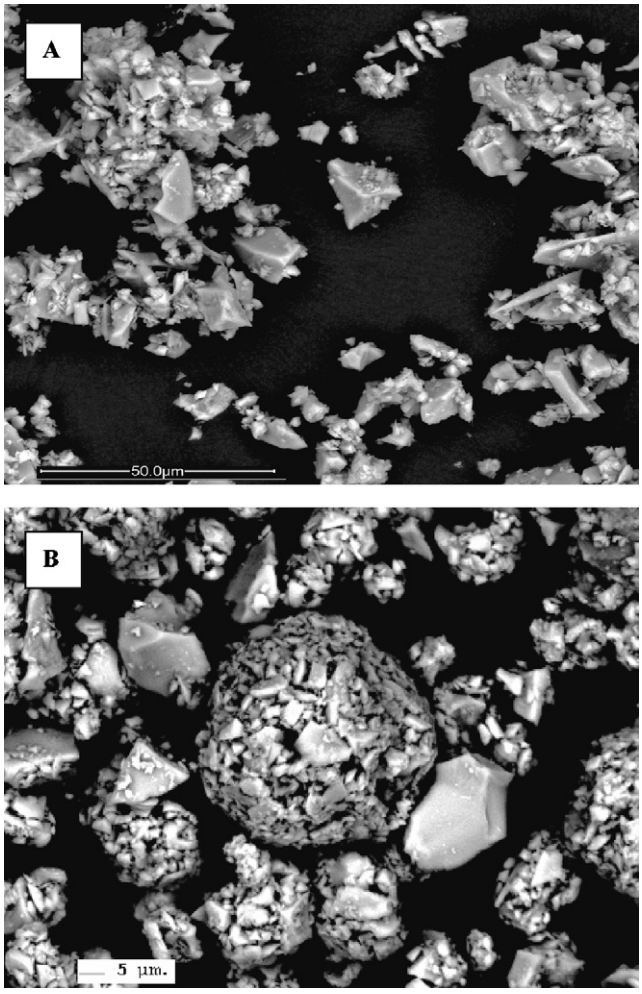

Fig. 2. SEM micrographs of CMAS: (A) ball-milled powder and (B) spray-dried powder.

3.2. Bulk glass samples characterization

The coefficients of thermal expansion (CTE, $100\,^{\circ}C < T < 600\,^{\circ}C$) of BAS glass is $8.27 \times 10^{-6}\,^{\circ}C^{-1}$, for CMAS glass is $7.72 \times 10^{-6}\,^{\circ}C^{-1}$, whereas, for CZAS glass is $8.25 \times 10^{-6}\,^{\circ}C^{-1}$. BAS and CZAS CTE values are quite similar to typical porcelanized stoneware value ($8.5 \times 10^{-6}\,^{\circ}C^{-1}$), instead CMAS one is lower. XRD characterization on the surface of BAS bulk glass sample after thermal treatment shows the crystallization of two phases (Table 5): hexacelsian as main phase ($Ba_{0.808}(Al_{1.71}Si_{2.29})O_8$, JCPDS 088-1050) and celsian ($BaAl_2Si_2O_8$, JCPDS 018-0153). CZAS samples treated at 1037 °C crystallized wollastonite-1A ($CaSiO_3$, JCPDS 084-0654) as main phase and wollastonite-2*M* ($CaSiO_3$, JCPDS 043-1460) on their surface. In the CMAS crystallized sample, peaks of anorthite ($CaAl_2Si_2O_8$ JCPDS 01-073-0265) as main phase and of diopside ($CaMgSi_2O_6$ JCPDS 025-0154) are clearly present. The crystallized thickness was around 250 μm

Table 5
Degree of crystallization of the samples and crystalline phases

CMAS sample	Degree of crystallization	Crystalline phases
As-sprayed	None	–
Coating T_{step1}	Low	Anorthite, diopside
Coating $T_{step1} + T_{step2}$	High	Anorthite, diopside
Sintered T_{step1}	Low	Anorthite, diopside
Sintered $T_{step1} + T_{step2}$	High	Anorthite, diopside
Crystallized bulk	On surface (few μm)	Anorthite, diopside
BAS sample	**Degree of crystallization**	**Crystalline phases**
As-sprayed	None	–
Coating T_{step1}	Low	Hexacelsian, celsian
Coating $T_{step1} + T_{step2}$	High	Hexacelsian, celsian
Sintered T_{step1}	Low	Hexacelsian, celsian
Sintered $T_{step1} + T_{step2}$	High	Hexacelsian, celsian
Crystallized bulk	On surface (250 μm)	Hexacelsian, celsian
CZAS sample	**Degree of crystallization**	**Crystalline phases**
As-sprayed	None	–
Coating T_{step1}	None	–
Coating $T_{step1} + T_{step2}$	Low	Wollastonite 1A, wollastonite 2M, anorthite (minor phase)
Sintered T_{step1}	None	–
Sintered $T_{step1} + T_{step2}$	Low	Wollastonite 1A, wollastonite 2M
Crystallized bulk	On surface (few μm)	Wollastonite 1A, wollastonite 2M

in the CZAS 15 mm thick sample; while in the BAS and CZAS ones, it was just around few microns (Table 5). Probably, CMAS glass devitrifies more easily than the other frits due to a higher tendency to crystallization. Therefore, crystallization in bulk samples, in all cases, occurs only on the surface and not in the whole specimen, making the manufacturing of a glass ceramic material almost impossible.

3.3. Single splats characterization

The characteristics of single splats, keeping constant the substrate on which they are collected, strongly depend on the process parameters (plasma flame temperature, velocity of the gases, distance from the substrate, etc.), on the quenching phenomena occurring on the substrate and on the coating material properties. All these causes are deeply correlated. The following observations are mainly phenomenological and qualitative, being quantitative measurements out of the aim of this paper, but they will be subject of future, further research.

Two broad types of glass splat morphologies have been identified in the samples of all the three frits, obtained with only one pass of the torch: pancake-like and flower-like shape.[16] Fig. 3C illustrates these morphologies. Pancake-like shape is typical for well-melted particles that flatten completely before solidification. These particles usually achieve good adhesion on the substrate. From an overhead view they present a circular shape. Instead, flower like shape is typical for overheated particles (near vaporization temperature), particles impacting with excessively high kinetic energy or particles which start solidification before complete spreading. When they impact on the substrate, they create radial fine droplets of material: thus, the shape of the splat is very irregular.[17–21] In the micrographs, the mushroom-like shape, characterized by a un-melted core and an external circular zone,[16] is absent. Probably, this is related to glassy nature of these coating materials: for temperature higher than T_g, viscosity can be low enough to get a good flattening.

If the splats have a large size, quenching stresses generate cracks inside the splats,[22] as can be noticed in Fig. 3. All kind of splats show a large number of pores, which can be one of the main causes of the high defectiveness of as-sprayed coating (paragraph 3.4.1). All three frits present the same two splats morphology but their distribution on the substrate is different (Fig. 3A–C). The difference in splats distribution depends on frits viscosity during deposition: in fact, at $T > T_g$, viscosity strongly influences the flowability of glassy materials. CZAS samples present less pores in the splats than the other frits (Fig. 3C) and the local composition of the splats is quite homogenous. In BAS e CMAS single splats samples, instead, local compositional differences can be noticed in backscattered electron micrographs, where the lighter areas indicate a higher amount of barium (Fig. 3A) and calcium (Fig. 3B), respectively. As expected, such phenomenon is still present if more layers are deposited and thick coatings are built (see Section 3.4.1).

3.4. Coatings characterization

3.4.1. Microstructure of the as-sprayed coatings

The as-deposited coatings are all thicker than 300 μm (Fig. 4). Similarly to crystalline ceramic plasma sprayed coatings (hard oxides, for example), they are characterized by often interconnected microcracks induced by relaxation of thermal stresses.[23–26] As expected, the porosity is mostly open and irregular, while it assumes a globular shape mainly because of gas entrapment during the deposition process and, maybe, because

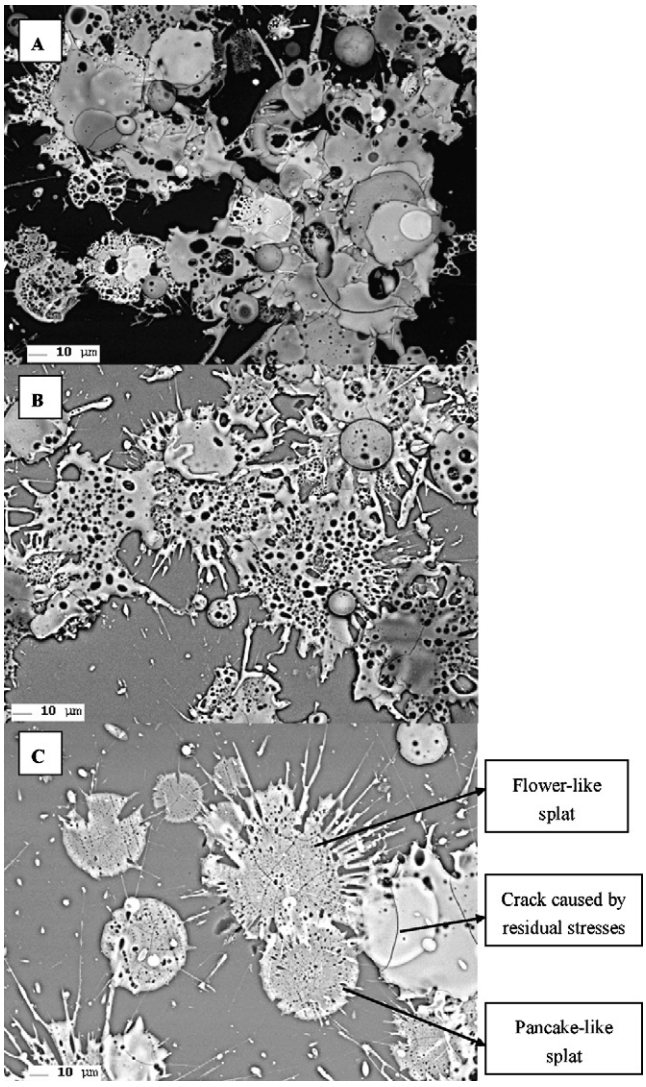

Fig. 3. Micrographs of single splats samples for BAS (A), CMAS (B) and CZAS (C).

of a local high degree of glass flowing caused by the overheating of previously deposited layers induced by the impinging particles or the plasma flame. For these reasons, such coatings are not watertight. Interlamellar porosity, probably due to the relatively low velocity of the impinging particles in the plasma jet,[27,28] is also present. Porosity measurements by image analysis show high values for all the three coatings: BAS = (18 ± 1)%; CMAS = (14 ± 3)%; CZAS = (13 ± 2.5)%. In these cases, nevertheless, the coating materials are glasses, whose viscosity can be low enough to allow deformation or coalescence of splats even if the temperature is far from the melting point. Thus, the typical lamellar structure and the splats boundaries are clearly identified only if local compositional differences have been induced during the deposition and lamellar solidification process, as quite clear in BAS and CMAS samples backscattered electron micrographs (Fig. 5A and B), where the lighter areas indicate a higher amount of barium and calcium, respectively. Plasma spraying is a process where thermal energy is strongly involved[3]: when the torch passes over and over the sample building the coating, it

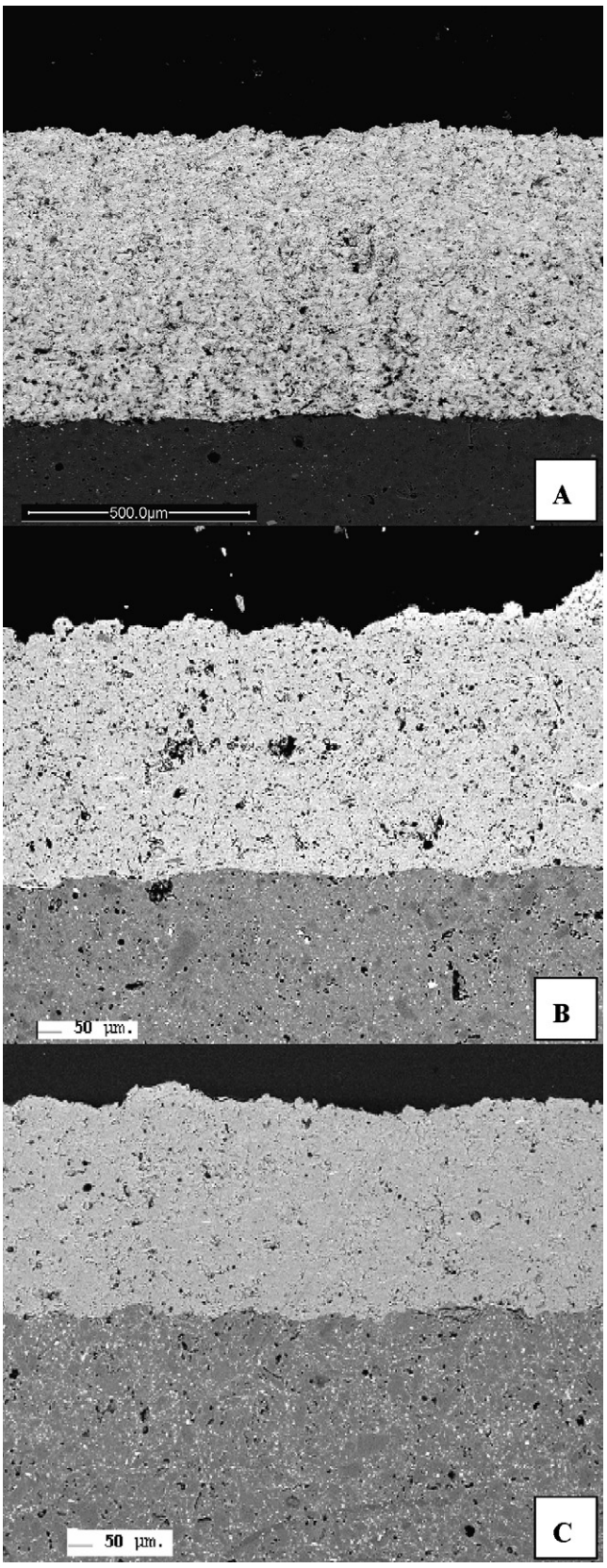

Fig. 4. SEM micrographs (backscattered electrons), cross-section; (A) BAS as-sprayed, (B) CMAS as-sprayed and (C) CZAS as-sprayed.

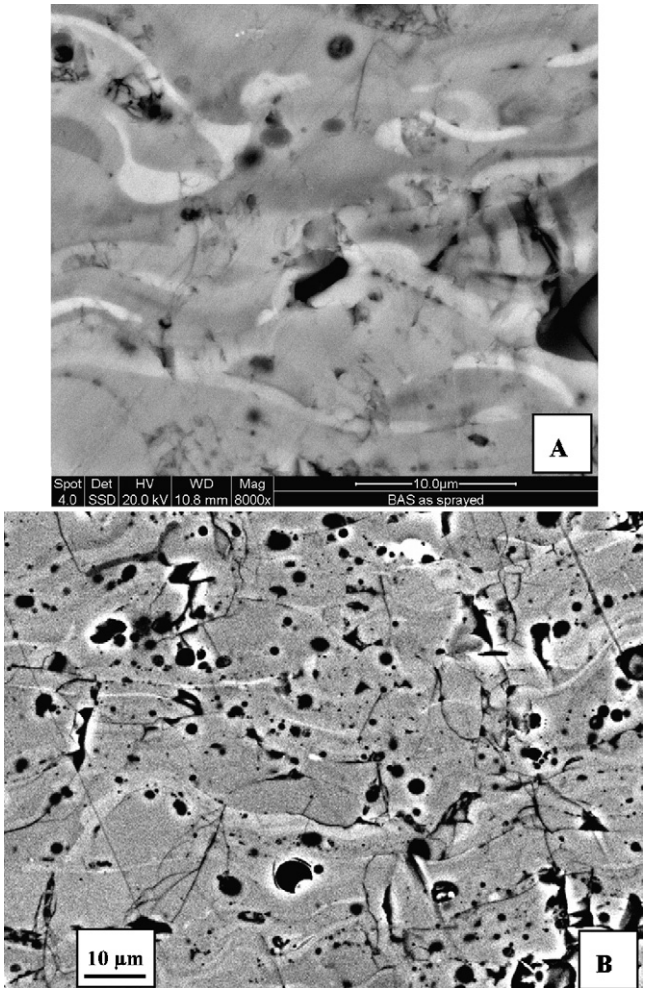

Fig. 5. Details of SEM micrographs (backscattered electrons), cross-section; (A) BAS as-sprayed and (B) CMAS as-sprayed.

can heat the surface causing local diffusion along splat boundaries. A very rapid quenching of the splats keeps the coating in a vitreous state, preventing devitrification, as demonstrated by XRD analysis (Fig. 6 curve A, Table 5).

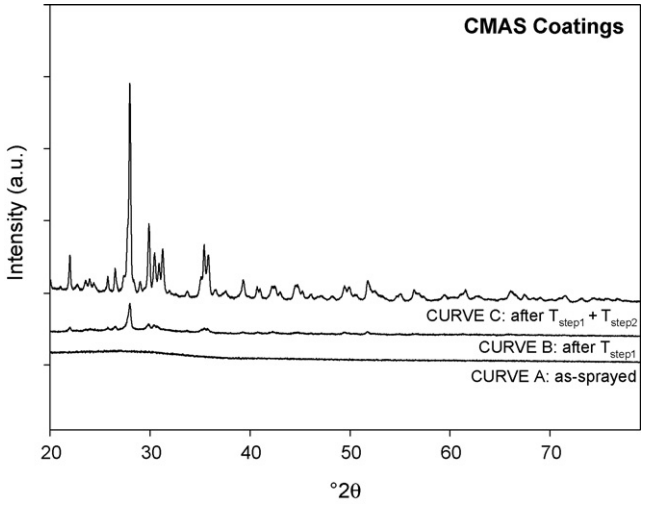

Fig. 6. XRD patterns of as-sprayed and thermally treated CMAS coatings.

3.4.2. Microstructure of the thermally treated coatings

The "as-sprayed" condition can be considered a sort of "pre-sintering" state, because many microstructural flaws are present, but the cohesion of the coating and its adhesion to the substrate are much higher than untreated glass powder simply pressed on a substrate. In Table 5, a global view of the qualitative crystallization degree reached by the various samples and the crystalline phases formed in the "as-sprayed" condition and after thermal treatment are shown.

Because of the crystallization behaviour of the BAS composition, it has been impossible to separate the sintering from the crystallization process (Table 5). Heterogeneous nucleation of hexacelsian (main phase) and celsian (monoclinic structure) took place, especially around pores, through the whole thickness of the coatings, at T_{step1}. Thus, at that temperature, a concurrent formation of crystals prevented closing the porosity, even if some cracks have been closed (Figs. 7A and 8A). The open porosity remained quite high ($9.5 \pm 0.5\%$). Besides, notwithstanding the good matching between the CTE of the substrate and the coating, the interface is heavily damaged with a crack running all along it (Fig. 8B). This latter phenomenon is another consequence of the overlapping of sintering and crystallization, as the glass is prevented from flowing and conforming easily to the substrate at the interface. The abovementioned behaviour of the coatings clearly demonstrate that, in order to consistently change the microstructure from the "as-sprayed" state to a well sintered one, no major crystal growth must take place while performing the sintering isotherm. For the same reasons, the crystallization treatment of BAS at $T_{step1} + T_{step2}$ has not brought any significant microstructural improvement (Fig. 9A; porosity, $(15 \pm 3)\%$).

In CMAS and CZAS cases, the treatment at T_{step1} induced a good sintering, decreasing and closing the porosity (CMAS = $6.5 \pm 0.5\%$; CZAS = $3.5 \pm 0.5\%$), eliminating the cracks and improving the interface with the substrate (Fig. 7B and C). In both CMAS and CZAS cases, the crystallization process has not significantly interfered with sintering (Fig. 6 curve B for the CMAS case).

After the double isotherm treatment, in CMAS the two main phases were diopside and anorthite (Table 5). In CMAS, the growth of crystals occurred after the flowing of the glass at the substrate interface. Thus, diopside and anorthite developed at the interface and the adhesion of the coating, which was mainly mechanical after spraying, became also chemical (Fig. 10). A moderate but not negligible increase of porosity ($11 \pm 1\%$) has been recorded in the CMAS coatings after significant devitrification (Fig. 9B), but it has not been possible to establish if or which of the two crystalline phases played the main role in the phenomenon, being deeper and further studies needed. As far as the CZAS composition is concerned, in the preliminary tests it was found that if the soaking time at the second isotherm was kept too long or the isotherm temperature was too high, a dramatic increase of porosity was observed (Fig. 11), together with the formation of wollastonite and anorthite, with $Ca_2ZrSi_4O_{12}$ as minor phase. The CZAS frit has been manufactured adding alumina to a CZS glass system. In a previous paper,[29] a CZS glass was plasma sprayed and heat treated under

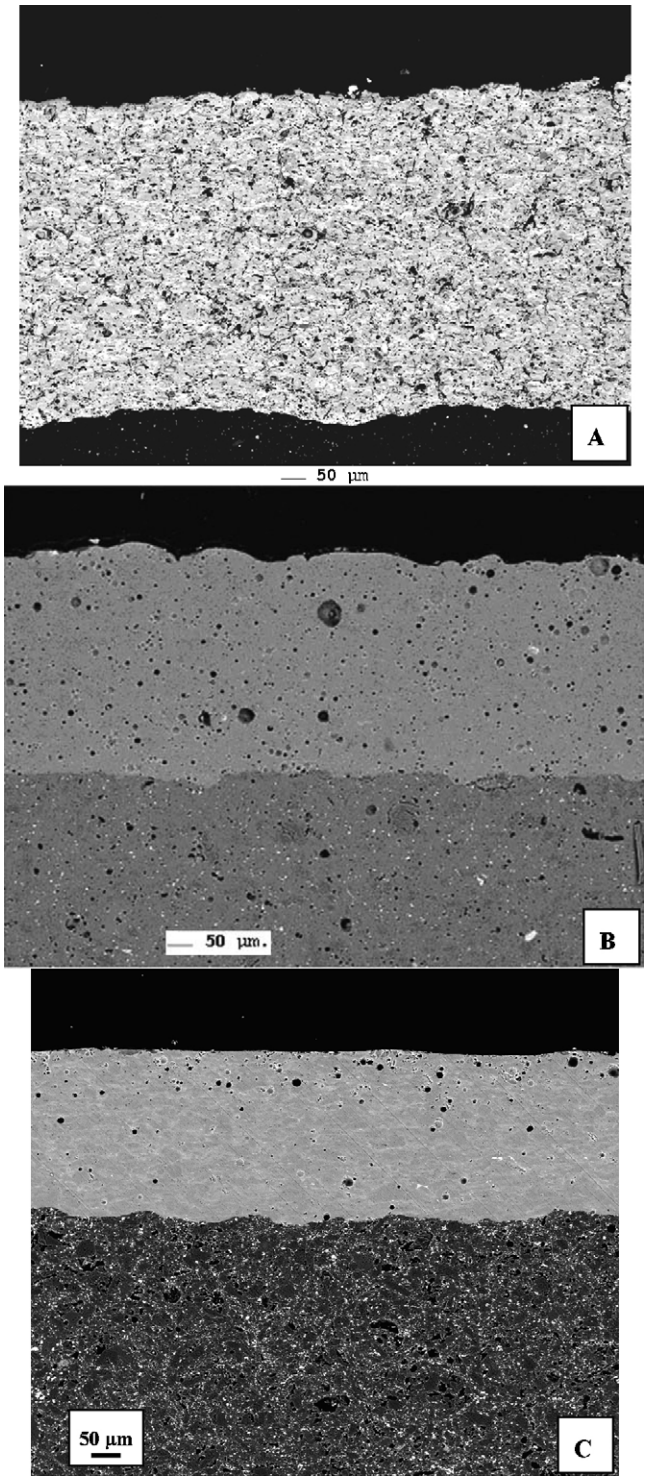

Fig. 7. SEM micrographs, cross-section; (A) BAS T_{step1}, (B) CMAS T_{step1} and (C) CZAS T_{step1}.

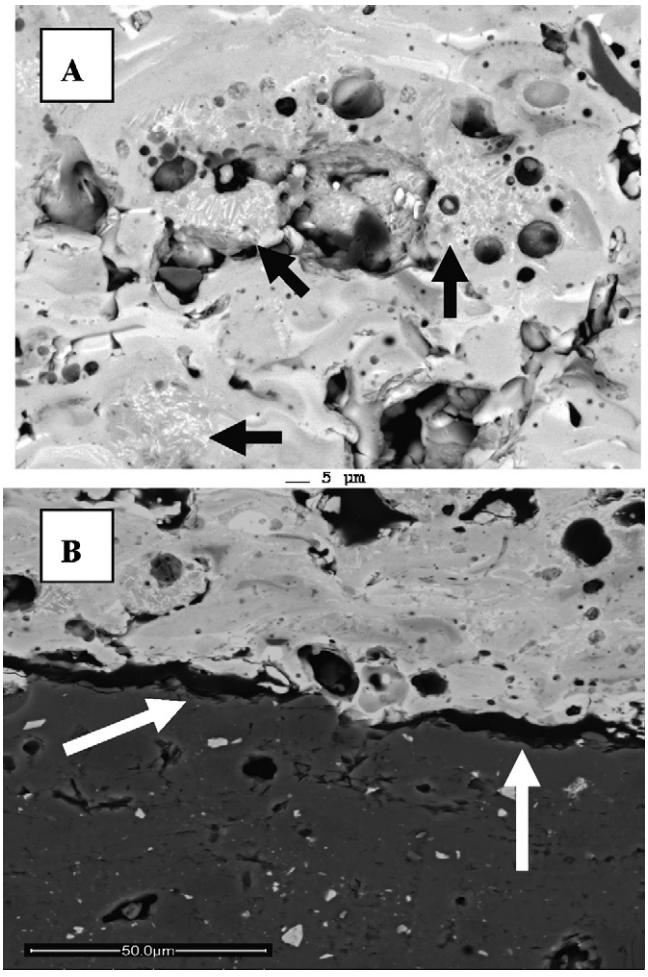

Fig. 8. SEM micrographs (backscattered electrons), details of cross-sections; BAS coating treated at T_{step1}: (A) black arrows indicating celsian crystals close to pores and (B) white arrows indicates a crack running along the interface.

similar conditions, without any significant increase of porosity. The present CZAS system has been obtained by adding alumina to the former CZS composition. While the CZS system formed wollastonite and $Ca_2ZrSi_4O_{12}$ as main crystalline phases, the CZAS mainly forms wollastonite and anorthite. Thus, the formation and growth of anorthite is likely to be the cause of this detrimental change in the microstructure, which can become uncontrolled. Thus, a "flash" treatment at 950 °C (the temperature has been just reached, no isotherm) has been performed (porosity = 6 ± 1%) to avoid the worsening of the microstructure of CZAS coatings (Fig. 9C): unfortunately, the considerably reduced formation of anorthite was associated with a overall low degree of crystallization, which became a major drawback. The main crystalline phases obtained with this thermal treatment are again wollastonite in the two forms (1A and 2M).

3.5. Sintered glass samples characterization

Considering CMAS, sample treated at T_{step1} shows a quite high degree of crystallization (anorthite and diopside) and a lower porosity (5%) than the coating treated at the same temperature (7% due to high defectiveness of the starting as-sprayed samples). The crystalline phases forming after the double isotherm treatment ($T_{step1} + T_{step2}$) occur also in the thermally treated coatings (anorthite and diopside). The porosity is about 8%, lower than the coating case (11%). Pore size is very small (<10 μm); the sample shows a good degree of sintering and crystallization occurred in its whole volume (heterogeneous nucleation likely occurred). BAS sintered glass samples show

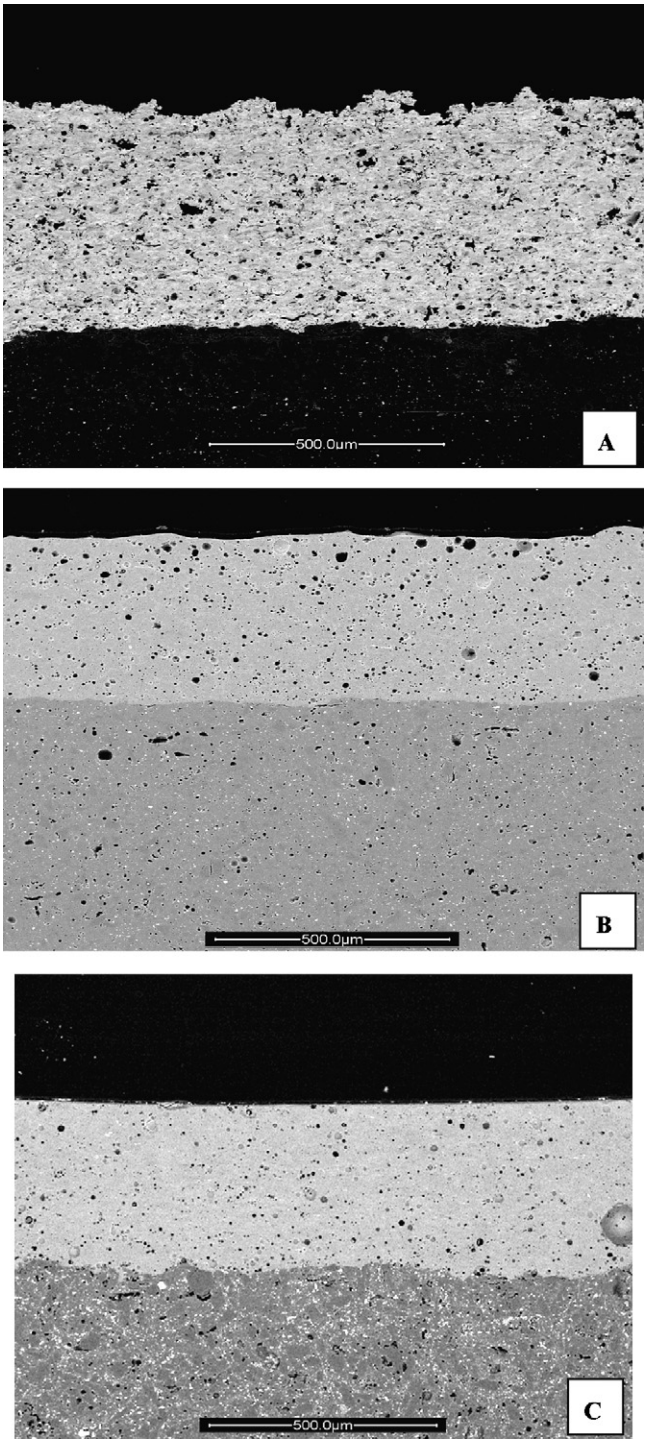

Fig. 9. SEM micrographs, cross-section: (A) BAS $T_{step1} + T_{step2}$, (B) CMAS $T_{step1} + T_{step2}$ and (C) CZAS $T_{step1} + T_{step2}$.

the same problems as coatings: a good sintering cannot be achieved. Thus, the samples show a low cohesion and very high porosity: a microstructure more similar to pressed powder than a sintered system. The porosity of the single isotherm treated sample is about 13%. CZAS sample treated both with single and double isotherm has a very low porosity and very small pores, about 1%, due to the high cohesion reached by sintering. In the CZAS sintered sample treated with double isotherm, the

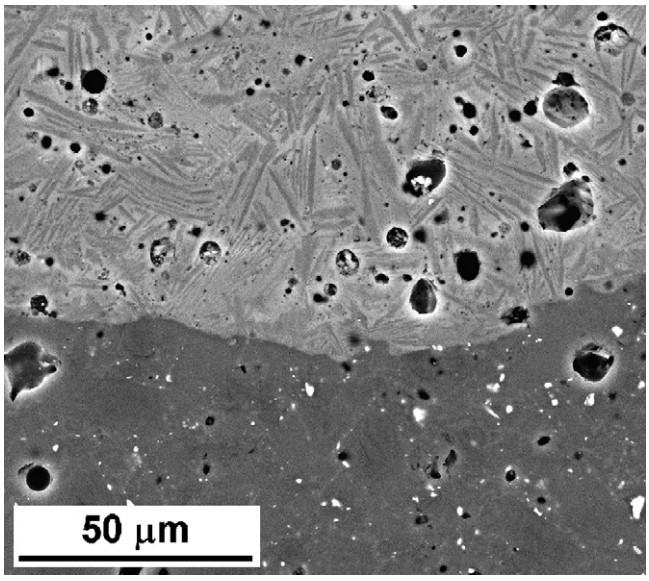

Fig. 10. Diopside and anorthite crystals developed at the interface with the substrate in CMAS coating treated at $T_{step1} + T_{step2}$.

crystallization degree is very low, due to the very short soaking time at T_{step2}: indeed, the same problem related to anorthite crystallization was also observed in sintered CZAS samples (Table 5).

3.6. Mechanical properties

3.6.1. Vickers microhardness

Fig. 12 indicates Vickers microhardness for the different specimens. Considering the bulk samples of the three frits, their microhardness are always higher than in the as-sprayed coatings case: in fact, a cast bulk glass has the highest cohesion possible. On the contrary, in a material which does not have an ideal cohesion, weak links can collapse and cause higher deformation as in the case of the untreated coatings, whichever the tested composition. Considering CMAS coatings, it can

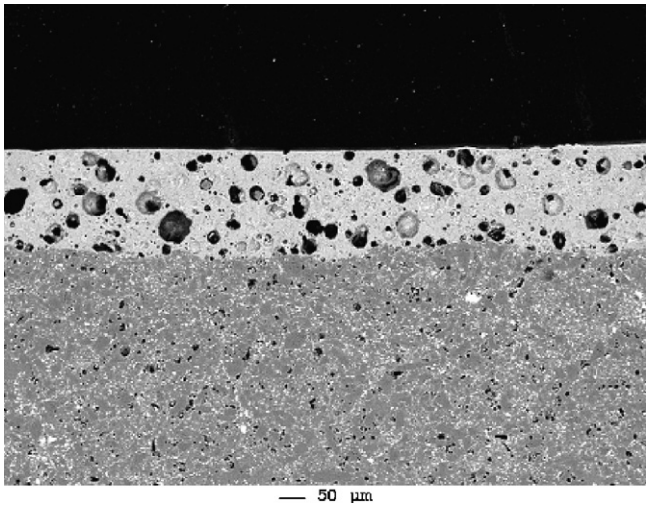

Fig. 11. SEM micrograph (backscattered electrons), cross-section; CZAS treated at 900 °C for 30 min + 1050 °C for 30 min.

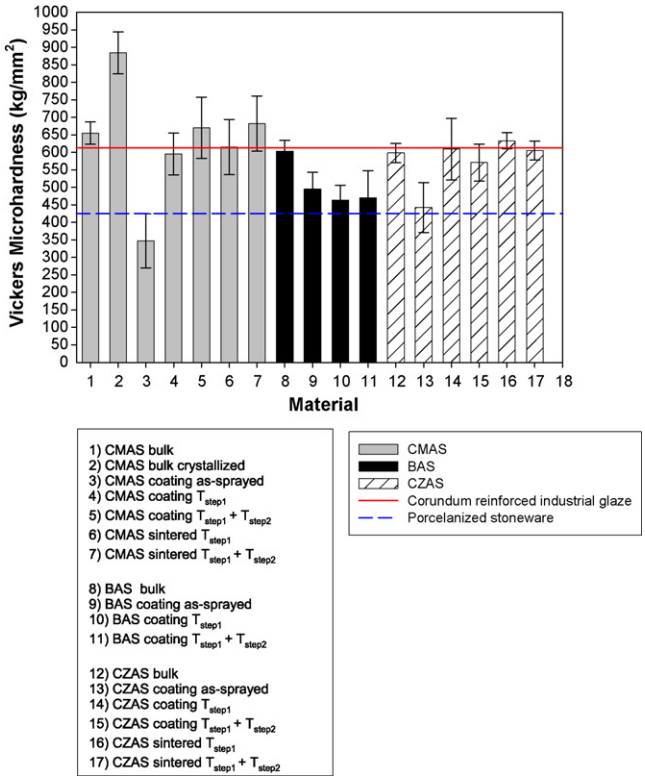

Fig. 12. Vickers microhardness (load = 0.25 N) for coatings, sintered and bulk.

be noticed that the coating treated with the double isotherm process is harder than the one treated with a single isotherm process. In particular, the coating treated at $T_{step1} + T_{step2}$ has a slightly higher microhardness than the bulk glass sample and the industrial high-performance glaze, probably because the formation of a glass ceramic "composite" microstructure significantly strengthens the material. The enhanced cohesion of the coatings also improved its hardness. Nevertheless, crystallized bulk glass has higher microhardness than the crystallized coating (since it has no defects), but the crystallization of the bulk involved just the first 250 μm of the sample thickness. Single and double isotherm treated coating hardness values are quite similar to values obtained for the corresponding sintered samples.

In the BAS case, even if a good crystallization is achieved, the cohesion is very low due to incomplete sintering, therefore hardness never overcomes that of the bulk glass nor that of the high performance glaze. Thus, in order to improve mechanical properties of a plasma sprayed glass ceramic coating, before inducing crystallization, it is necessary to enhance its microstructure through a good sintering. Hardness was not measurable on sintered BAS samples, because the cohesion is too poor to allow proper indentations to be performed, due to the above-mentioned overlapping of sintering and crystallization. For the same reason, hardness values obtained for as-sprayed and thermally treated coatings are quite similar.

After the treatment at T_{step1}, CZAS coatings are very well sintered and the hardness has greatly improved. Double isotherm treatment produced only a limited crystallization that does not enhance hardness and produces also a more defective microstructure worsening the coating cohesion (both in the coatings and glass sintered samples), probably because of anorthite formation. However, it is very important to notice that all the thermally treated coatings of the three frits have higher microhardness than porcelanized stoneware.

3.6.2. Fracture toughness

Fig. 13A and B indicate indentation fracture toughness for the different materials calculated with the two different

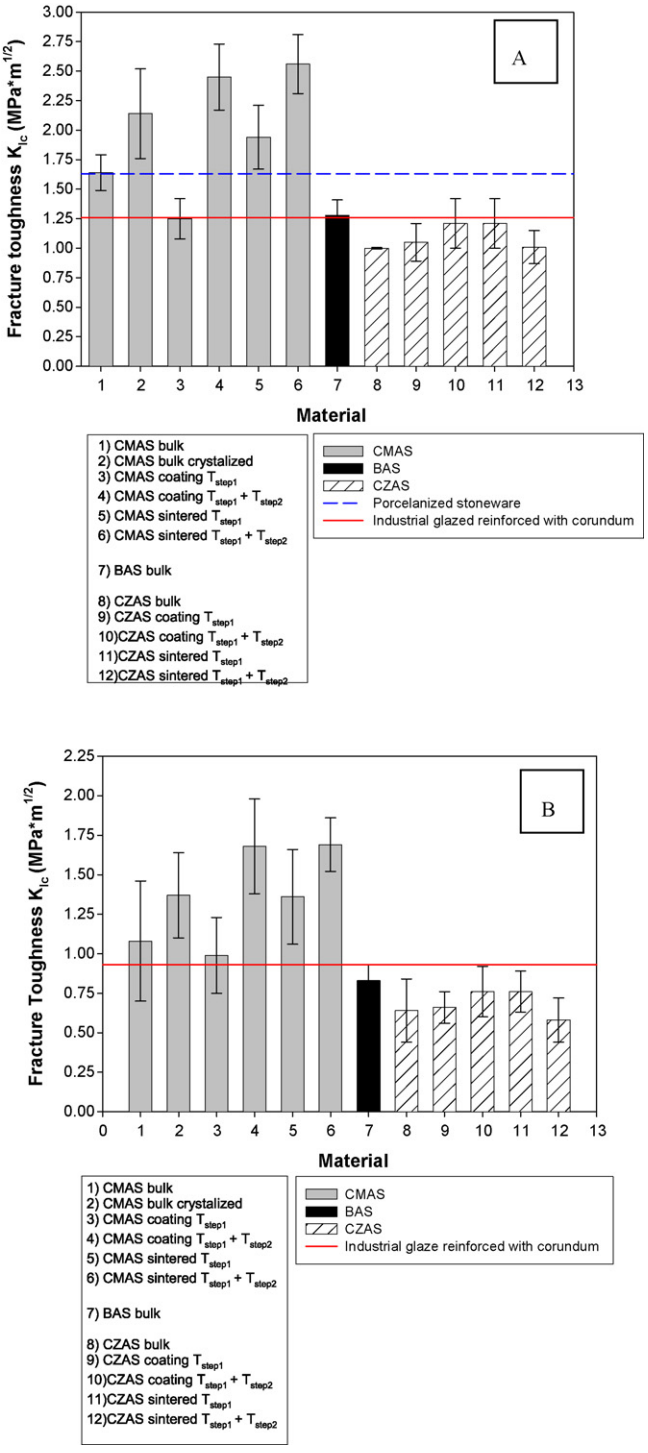

Fig. 13. Fracture indentation toughness for the different materials calculated with Evans–Charles (A) and Evans–Wilshaw (B) formulas.

formulas. The absolute values are different, but the relative trends do not change. Fracture toughness is strongly dependent on microstructure and less on structure than microhardness, because microstructural features can significantly affect stresses distribution in a material, and hence, alter cracks formation and propagation. Therefore, a material with many pores and defects will be less though than a dense material, while the presence of reinforcing phases will help increasing toughness. Higher K_{IC} values measured for bulk glass samples can been explained by the above-mentioned consideration, because, thanks to their excellent cohesion, their microstructure does not present significant defects. Porcelanized stoneware has high toughness too, because it has a compact microstructure and it is reinforced by crystalline phases as quartz and mullite. The toughness could not be measured by indentation on as-sprayed samples: the presence of many microcracks and pores and the low cohesion of the coating did not allow an acceptable reading of the cracks induced by the Vickers diamond tip.

The microstructure of CMAS coating heated at T_{step1} shows a relatively high residual porosity without crystalline phases to reinforce the material, so it has lower K_{IC} than porcelanized stoneware. The toughness value for the corresponding sintered sample treated at T_{step1} is higher than the coating value, because it has a more compact microstructure (lower porosity). CMAS coating thermally treated at $T_{step1} + T_{step2}$ has a good fracture toughness, higher than porcelanized stoneware, bulk glass samples and industrial glaze, because of the formation of anorthite and diopside crystalline phases in the whole coating thickness. Moreover, in order to induce a measurable cracking by indenting, a higher load (6 N) than in all other tests had to be exceptionally chosen. The potential benefits offered by crystallization are fully exploited, because frequent crack deflections due to several small crystals obstacle crack propagation and increase K_{IC} of the coating.

BAS microstructure was still defective after the thermal treatments: both for coatings and for sintered samples, toughness was experimentally not measurable, because multiple cracking and material crushing under the indenter occurred due to the poor cohesion. BAS bulk has a toughness value comparable with industrial glaze one.

Considering CZAS coating treated at T_{step1}, even if the microstructure is very good (due to full sintering), K_{IC} is still low both for coating and sintered samples, since no toughening by crystalline phases occurs. Heat treatment at $T_{step1} + T_{step2}$ does not significantly improve the toughness of CZAS coatings, remaining much lower than the typical values recorded on porcelanized stoneware, because they are not fully crystallized and the few crystals are unable to reinforce the material. Nevertheless, thanks to them and to the improvement of the microstructure, according to the Evans-Charles formula, the indentation fracture toughness was increased almost up to the typical values recorded on a high quality glaze.

3.6.3. Deep abrasion resistance

Fig. 14 indicates the deep abrasion resistance for all tested coatings, glaze and stoneware. All kind of as-sprayed coatings have a quite low abrasion resistance, being the wear volume

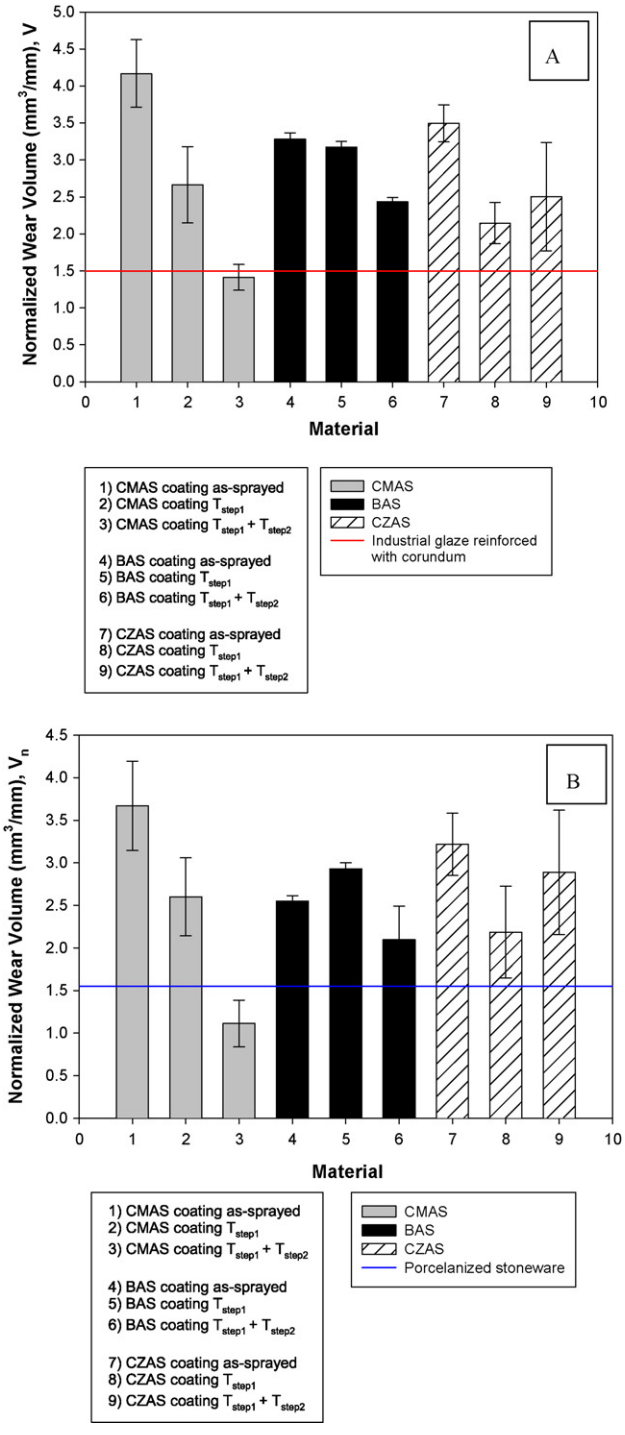

Fig. 14. Abrasion resistance for the different materials: (A) V_{mm} at seven laps and (B) V_{mm} average (7, 14 and 21 laps).

at least twice than the one measured for the industrial glaze (Fig. 14A). Well sintered coatings (CMAS, CZAS) have a higher cohesion, indicated also by the hardness increase, but they still remain more brittle than porcelanized stoneware because their nature is still vitreous and no crystalline phases are present as reinforcements, as formerly noticed: thus, they still display lower abrasion resistance (Fig. 14B). The morphology of the abrasion track on CMAS coatings treated at T_{step1} observed through SEM micrographs (Fig. 15A) shows smooth fracture surfaces with

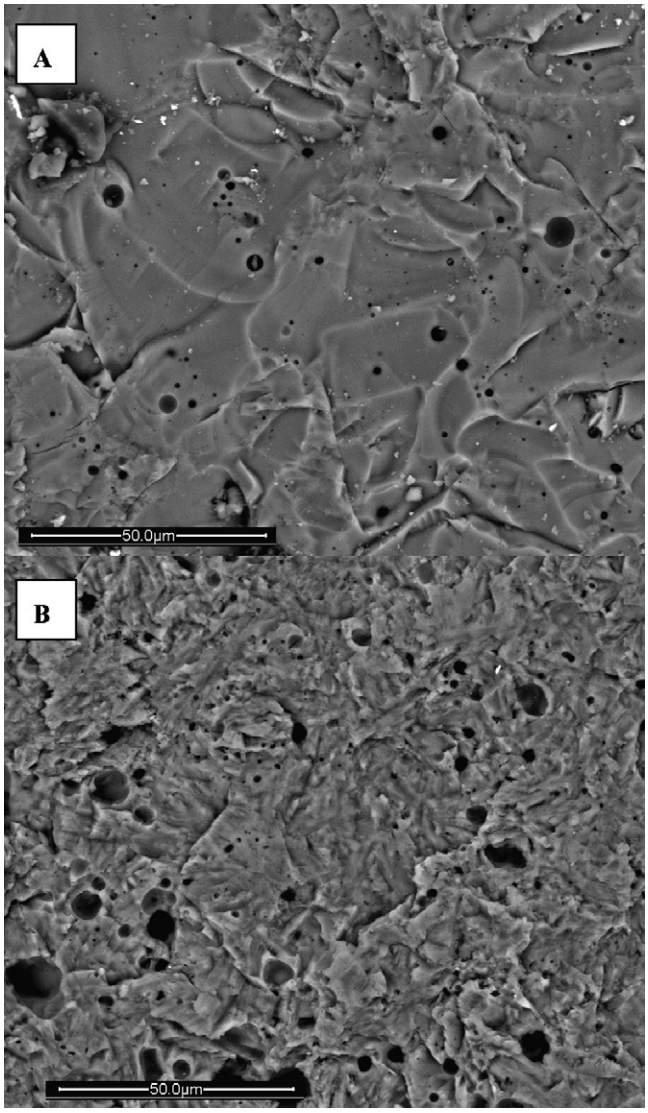

Fig. 15. Abrasion trace micrograph of thermally treated CMAS coatings: (A) T_{step1} and (B) $T_{step1} + T_{step2}$.

cracks propagating rather straightforwardly and undisturbed. BAS coatings treated at T_{step1} did not show any significant improvement because the microstructure was still defective and the crystallization degree still low (Table 5). It must be noticed that only CMAS treated at $T_{step1} + T_{step2}$ was more resistant than the industrial glaze and porcelanized stoneware, because it was fully devitrified becoming a glass ceramic coating: the presence of crystalline grains in samples treated at $T_{step1} + T_{step2}$ hinders crack propagation through the coating, enhancing abrasion resistance. In fact, the morphology of the abrasion track on CMAS coatings (Fig. 15B) is quite irregular with cracks, which appear to have undergone several deflections. This indicates that, as predictable, brittle fracture is the most important abrasion mechanism. Considering CZAS coatings after the $T_{step1} + T_{step2}$ treatment, abrasion resistance never exceeded the value measured for porcelanized stoneware because it was impossible to obtain at the same time their full crystallization and preserving the good microstructure reached through sintering (anorthite

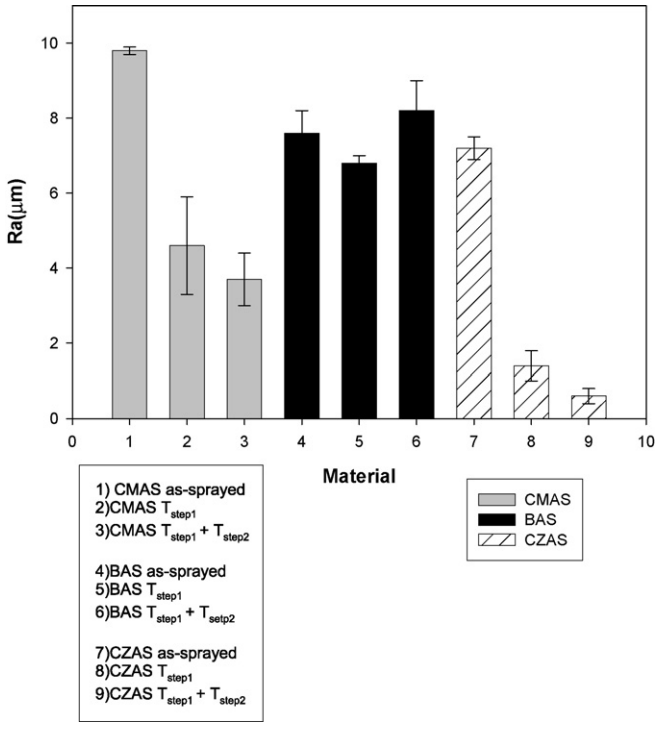

Fig. 16. Average roughness, R_a, of the samples.

crystal growth leads to an uncontrollable increase of porosity). BAS response to abrasion after the crystallization step is just slightly better than in the T_{step1} case, because of a higher degree of devitrification induced in the samples.

3.6.4. Roughness

Values of surface roughness obtained for both as-sprayed and thermally treated coatings for the three frits are listed in Fig. 16. Comparing CMAS and CZAS as-sprayed coating with their corresponding samples treated at T_{step1}, it can be observed that, in both cases, roughness is decreased by thermal treatment. During the sintering, glassy phase present in these samples reaches a quite low viscosity and the surfaces becomes smoother, producing a roughness decrease. This phenomenon is more evident in CZAS sample due to the high sintering degree reached. In BAS samples, average roughness has about the same values for as-sprayed and thermally treated coatings, because full sintering never occurs. In CMAS samples, the difference in roughness is very slight passing from coating treated at T_{step1} to coating treated at $T_{step1} + T_{step2}$, because at T_{step1} the coating already is very compact, thanks to the good sintering. Moreover, at $T_{step1} + T_{step2}$, solid crystal grains block the viscous flow of glassy phase. The possible difference in specific volume values between crystal phase and glassy phase may also wrinkle the samples surfaces.

4. Conclusions

Three different industrial frits have been successfully plasma sprayed on porcelainized stoneware tiles. The as-sprayed microstructures were fully vitreous and very defective: pores,

cracks due to thermal stresses relaxation and very rough and irregular surfaces were present. Post-process thermal treatment enhanced the microstructure in many cases, but the degree of improvement strongly depended on the thermal behaviour of the coating materials. A proper combination of sintering and crystallization allowed to fully exploit the coating material, changing it into a glass ceramic one, with micromechanical and wear properties comparable or superior to porcelainized stoneware and an high quality industrial glaze, taken as standard for comparison. Consequently, some general conclusions on plasma spraying of glass and glass ceramics coatings can be drawn. In the as-sprayed conditions the coatings are always defective (pores, inter- and intralamellar cracks) so they must be thermally treated to be comparable to glazes produced with standard techniques or to become watertight. In some applications, such as bioglasses, these post-process treatments could be not mandatory, because permeability to liquids and porosity are often required. In any case, proper heat treatments always improve the coatings mechanical properties. The highest improvement in mechanical properties is obtained when controlled crystallization of suitably chosen glass compositions is achieved. Particularly, full exploitation of the devitrification is successful only if sintering and crystallization do not overlap significantly. Moreover, the kind of crystalline phases, hence, the mother glass composition, must be carefully chosen, because their formation can sometimes induce an unacceptable increase of porosity. Thus, future developments of this research will focus on the formulation of glass compositions, whose properties have to match the two latter points, in order to achieve very high quality glass ceramic coatings (small amount of porosity, high toughness induced by crystallization). Other further developments concern a more detailed study in order to correlate spray conditions, glass properties (viscosity, surface tension, etc.) and resulting splat and coating microstructure.

Acknowledgement

Thanks to Ing. F. Casadei, Mr. E. Severini and Mr. V. Ferretti, for the plasma spray runs (Centro Sviluppo Materiali, Italy). The authors gratefully thank Dr. Antonella Sola and Prof. Federica Bondioli for the measurements of the thermal properties of the frits. Frits and glazed tiles by Colorobbia S.p.A. are acknowledged. Partially supported by PRRIITT (Regione Emilia Romagna), Net-Lab "Surface & Coatings for Advanced Mechanics and Nanomechanics" (SUP&RMAN).

References

1. Emiliani, G. P. and Corbara, F., *Tecnologia Ceramica—Volume II: La Lavorazione*. Gruppo Editoriale Faenza Editrice, Faenza, 1999, pp. 383–441.
2. Bolelli, G., Cannillo, V., Lusvarghi, L., Manfredini, T., Siligardi, C., Bartuli, C. *et al.*, Plasma-sprayed glass-ceramic coatings on ceramic tiles: microstructure, chemical resistance and mechanical properties. *Journal of the European Ceramic Society*, 2005, **25**, 1835–1853.
3. Crawmer, D. E., In *Handbook of Thermal Spray Technology*, ed. J. R. Davis. ASM International, Materials Park, OH, USA, 2004, pp. 62–69.
4. Schrooten, J. and Helsen, J. A., Adhesion of bioactive glass coating to Ti6Al4V oral implant. *Biomaterials*, 2000, **21**, 1461–1469.
5. Polzonetti, G., Iucci, G., Frontini, A., Infante, G., Furlani, C., Avigliano, L. *et al.*, Surface reactions of a plasma-sprayed $CaO–P_2O_5–SiO_2$-based glass with albumin, fibroblasts and granulocytes studied by XPS, fluorescence and chemiluminescence. *Biomaterials*, 2000, **21**, 1531–1539.
6. Olivia, A., Salerno, A. and Locardi, B., Behaviour of human osteoblasts cultured on bioactive glass coatings. *Biomaterials*, 1998, **19**, 1019–1025.
7. Goller, G., The effect of bond coat on mechanical properties of plasma sprayed bioglass-titanium coatings. *Ceramics International*, 2004, **30**, 351–355.
8. Gawne, D. T., Qiu, Z., Bao, Y., Zhang, T. and Zhang, K., Abrasive wear resistance of plasma-sprayed glass-composite coatings. *Journal of Thermal Spray Technology*, 2001, **10**(4), 599–603.
9. Bolelli, G., Cannillo, V., Lusvarghi, L. and Manfredini, T., Glass-alumina composite coatings by plasma spraying. Part I: microstructural and mechanical characterization. *Surface & Coatings Technology*, 2006, **201/1-2**, 458–473.
10. Bolelli, G., Cannillo, V., Lusvarghi, L., Manfredini, T. and Montorsi, M., Glass-alumina composite coatings by plasma spraying. Part II: microstructure based modeling of mechanical properties. *Surface & Coatings Technology*, 2006, **201**(1/2), 474–486.
11. Cannillo, V., Lusvarghi, L., Siligardi, C. and Sola, A., Characterization of glass–alumina functionally graded coatings obtained by plasma spraying. *Journal of the European Ceramic Society*, 2007, **27**(4), 1935–1943.
12. Bolelli, G., Lusvarghi, L., Manfredini, T. and Siligardi, C., Influence of The manufacturing process on the crystallization behaviour of a CZS glass system. *Journal of Non-Crystalline Solids*, 2005, **351**, 2537–2546.
13. Ang, C. B., Devasenapathi, A., Ng, H. W., Yu, S. C. M. and Lam, Y. C., A proposed process control chart for DC plasma spraying process. Part II. experimental verification for spraying alumina. *Plasma Chemistry and Plasma Processing*, 2001, **21**, 401–420.
14. Evans, A. G. and Charles, E. A., Fracture toughness determinations by indentation. *Journal of the American Ceramic Society*, 1976, **59**(7/8), 371–372.
15. Evans, A. G. and Wilshaw, T. R., Quasi-static solid particle damage in brittle solids—1. Observations, analysis and implications. *Acta Metallurgica*, 1976, **24**, 939–956.
16. Fan, X., Gitzhofer, F. and Boulos, M., Investigation of alumina splats formed in the induction plasma process. *Journal of Thermal Spray Technology*, 1998, **7**(2), 197–204.
17. Longo, F. N., In *Handbook of Thermal Spray Technology*, ed. J. R. Davis. ASM International, Materials Park, OH, USA, 2004, pp. 122–123.
18. Li, L., Vaidya, A., Sampath, S., Xiong, H. and Zheng, L., Particle characterization and splat formation of plasma sprayed zirconia. *Journal of Thermal Spray Technology*, 2006, **15**(1), 97–105.
19. Fukumoto, M., Nishioka, E. and Nishiyama, T., New criterion for splashing in flattening of thermal sprayed particles onto flat substrate surface. *Surface and Coatings Technology*, 2002, **161**, 103–110.
20. Fauchais, P., Fukumoto, M., Vardelle, A. and Vardelle, M., Knowledge concerning splat formation: an invited review. *Journal of Thermal Spray Technology*, 2004, **13**(3), 337–360.
21. Dhiman, R. and Chandra, S., Freezing-induced splashing during impact of molten metal droplets with high weber number. *International Journal of Heat and Mass Transfer*, 2005, **48**, 5625–5638.
22. Kuroda, S. and Clyne, T. W., The quenching stress in thermally sprayed coatings. *Thin Solid Films*, 1991, **20**, 49–66.
23. Deshpande, S., Kulkarni, A., Sampath, S. and Herman, H., Application of image analysis for characterization of porosity in thermal spray coatings and correlation with small angle neutron scattering. *Surface and Coatings Technology*, 2004, **187**, 6–16.
24. Antou, G., Montavon, G., Hlawka, F., Cornet, A. and Coddet, C., Characterizations of the pore-crack network architecture of thermal-spray coatings. *Materials Characterization*, 2004, **53**, 361–372.
25. Li, C. J. and Ohmori, A., Relationships between the microstructure and properties of thermally sprayed deposits. *Journal of Thermal Spray Technology*, 2002, **11**, 365–374.
26. Sevostianov, I., Kachanov, M., Ruud, J., Lorraine, P. and Dubois, M., Quantitative characterization of microstructures of plasma-sprayed coatings and their conductive and elastic properties. *Materials Science and Engineering A*, 2004, **386**, 164–174.

27. Herman, H., Sampath, S. and McCune, R., Thermal spray: current status and future trends. In *Thermal Spray Processing of Materials*, ed. S. Sampath and R. McCune. MRS Bulletin, 2000, pp. 17–25, July.
28. Kulkarni, A., Sampath, S., Goland, A. and Herman, H., Computed microtomography studies to characterize microstructure-property correlations in thermal sprayed alumina deposits. *Scripta Materialia*, 2000, **43**, 471–476.
29. Bolelli, G., Lusvarghi, L., Manfredini, T. and Siligardi, C., Devitrification behaviour of plasma-sprayed glass coatings. *Journal of the European Ceramic Society*, 2007, **27**(2/3), 623–628.